

# Supporting information for: Observation of room temperature photoluminescence blinking in armchair-edge graphene nanoribbons

Markus Pfeiffer,<sup>\*,†</sup> Boris V. Senkovskiy,<sup>‡</sup> Danny Haberer,<sup>¶</sup> Felix R. Fischer,<sup>¶</sup>  
Fan Yang,<sup>‡</sup> Klaus Meerholz,<sup>†</sup> Yoichi Ando,<sup>‡</sup> Alexander Grüneis,<sup>‡</sup> and  
Klas Lindfors<sup>\*,†</sup>

<sup>†</sup>*Department für Chemie, Universität zu Köln, Luxemburger Strasse 116, 50939 Köln,  
Germany*

<sup>‡</sup>*II. Physikalisches Institut, Universität zu Köln, Zùlpicher Strasse 77, 50937 Köln,  
Germany*

<sup>¶</sup>*Department of Chemistry, University of California at Berkeley, Tan Hall 680, Berkeley,  
CA 94720, USA*

E-mail: m.pfeiffer@uni-koeln.de; klas.lindfors@uni-koeln.de

## Experimental setup

The setup is an in-house developed fluorescence microscope. For spectrally integrated fluorescence micrographs we illuminate an area with a diameter of about 28  $\mu\text{m}$  of the sample by slightly focusing the incident beam to the back focal plane of the microscope objective. For spectral imaging a cylindrical lens is combined with the lens, which is used to focus the incident beam on the back focal plane of the objective, to form a beam expander. This

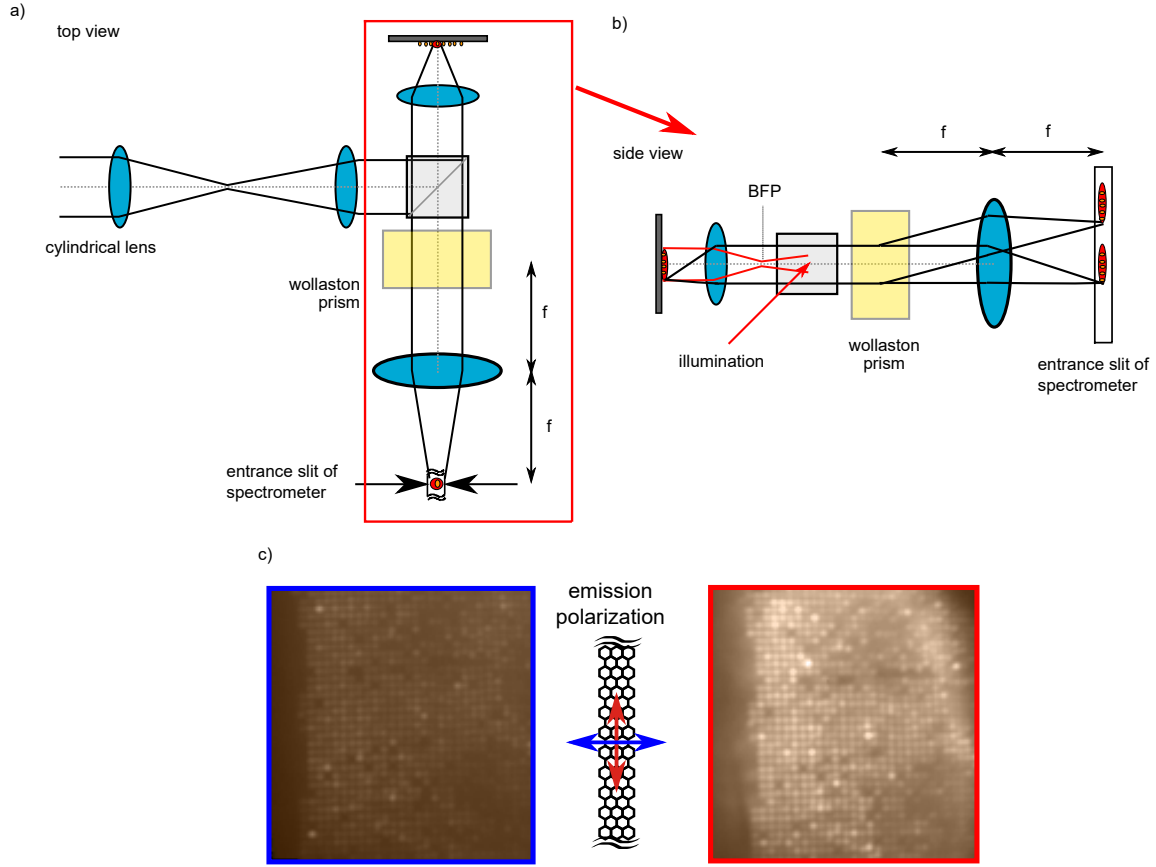


Figure S1: Sketch of the experimental setup used for spectral imaging. The top and side views are shown in a) and b), respectively. The sample is illuminated with an elliptical spot that is narrow in width in the direction of the spectrometer entrance slit. When the cylindrical lens is removed, one obtains wide-field illumination in both lateral directions. c) Polarization-resolved wide-field fluorescence micrographs.

results in a beam that is focused in only one direction entering the objective (see Fig. S1a–b). With this we achieve an elliptical illumination spot with large aspect ratio oriented along the direction of the entrance slit of the spectrometer. We are thus able to collect spectra from many nanoantennas simultaneously using the CCD detector in the spectrometer. In the emission path, we introduce a Wollaston prism at one focal length distance before the lens used to focus the emission into the spectrometer. This images the two polarization components spatially separated above each other (see Fig. S1b) and the emission for both polarization components are acquired simultaneously. Dielectric filters are used to separate the excitation light from the emission. For the spectrally integrated imaging the maximum

excitation intensity used is approximately  $100 \text{ W/cm}^2$ . For the spectral imaging, we estimate a maximum excitation intensity of below  $350 \text{ W/cm}^2$ .

The signal from isolated blinking spots was processed as follows: First a constant background was subtracted from the signal to remove the constant offset of the images and spectra acquired with the CCD camera. After this, the signal was divided with the average intensity of the wide-field micrographs (example in Fig. S1c) to reduce power fluctuations due to photobleaching and laser noise.

## Number of ribbon termini in hot spot

We use the simulated spatial pattern of the enhancement factor to estimate the number of ribbons whose termini lies in the regions of high enhancement factor (EF), i.e. in the hot spot. The spatial extent of the Tamm state along the ribbon is on the order of  $5 \text{ \AA}$ .<sup>1</sup> The hot spot is significantly larger. Thus the terminus can be assumed to be pointlike. Figure S2 shows histograms of the number of ribbon termini in the hot spot. For the calculations, GNRs are placed in rows with a period of  $3.8 \text{ nm}$ , which corresponds to the terrace spacing of the Au788 growth crystal.<sup>2</sup> Along each row, the GNRs have a constant separation of  $5 \text{ nm}$ . The relative position of the GNR termini between different rows is random. In Figure S2 we consider GNRs with  $30 \text{ nm}$  length (left panel) and  $40 \text{ nm}$  (right panel). The histograms are an average from 1000 random ribbon configurations. In the vicinity of the nanoantennas we have many GNRs. Therefore, in order to observe a single one, the GNR with its terminus in the hot spot must have an enhanced signal comparable to that of all the other ribbons together.

In Figure S2 we show the number of GNR termini in the hot spot. The histograms are in good agreement with experimental observations. We observe that in most cases we have no GNRs in the hot spot. For approximately 20 % of the antennas, we find one GNR terminus in the hot spot, and very occasionally we obtain two or more. The calculated signal contrast

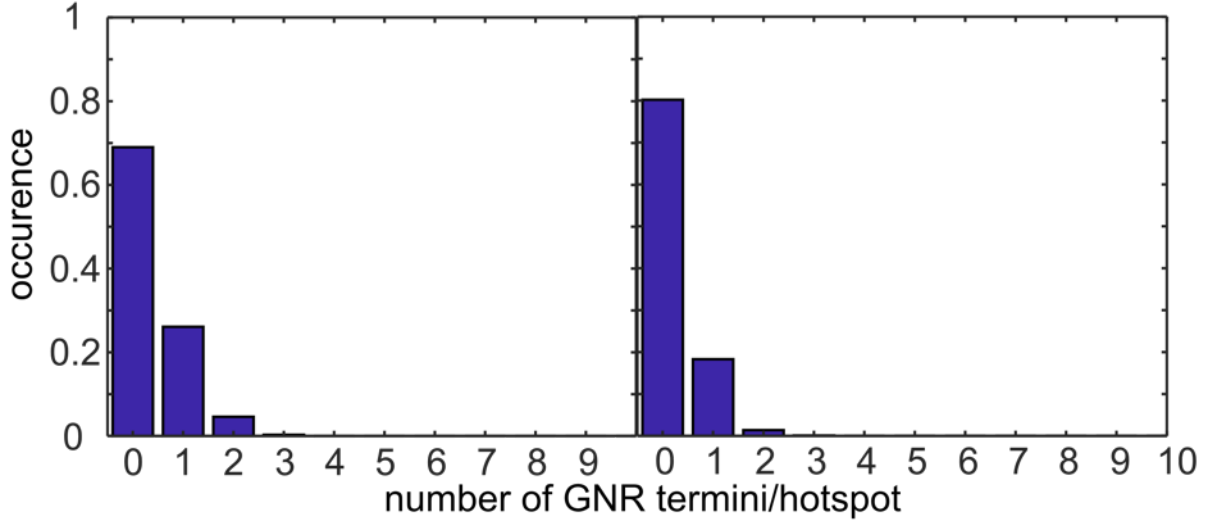


Figure S2: Histogram for the number of strongly enhanced GNRs per hot spot. In the left panel the threshold for the hot spot is 75 % of the largest enhancement factor (EF). In the right panel the threshold EF is 400 (81 % of the largest EF). A transfer efficiency of 100 % is assumed. For the lateral separation, we use the spacing of the Au788 terraces of 3.8 nm. The distance along the GNRs is assumed to be 5 nm. For the calculations a GNR length of 40 nm (left panel) or 30 nm (right panel) is assumed.

between the single highly enhanced ribbon and the ensemble signal of all the other GNRs is also in good agreement with the experiment. For example, for the case shown in Figure 1 in the right panel, where the threshold for the selection of the GNRs in the hot spot is  $EF > 400$  (81 % of the largest EF), the signal of the highly enhanced single ribbon is approximately 30 % of the ensemble signal. In the experiment (see Fig. 1e in the manuscript) the contrast shows a comparable magnitude.

## Additional measurements and data

### Ambient pressure

The dataset presented in the main text in Fig. 2 consists of 200 spectra. Here we show in Fig. S3 an exemplary spectrum (blue) from this dataset. The peak visible in the spectrum was fitted with a Lorentzian peak yielding a spectral width of 49.9 meV. The integration time was 2 s. The resonance spectrum of the antennas is visible in the extinction spectrum

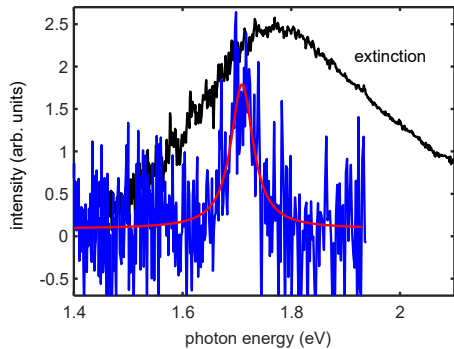


Figure S3: Single emission spectrum (blue) from dataset from Fig. 2 in main text with an integration time of 2 s. The spectral width of the fitted Lorentzian function (red) is 49.9 meV. The extinction spectrum [1-transmission (1-T)] of the plasmonic antennas (black) display a resonance.

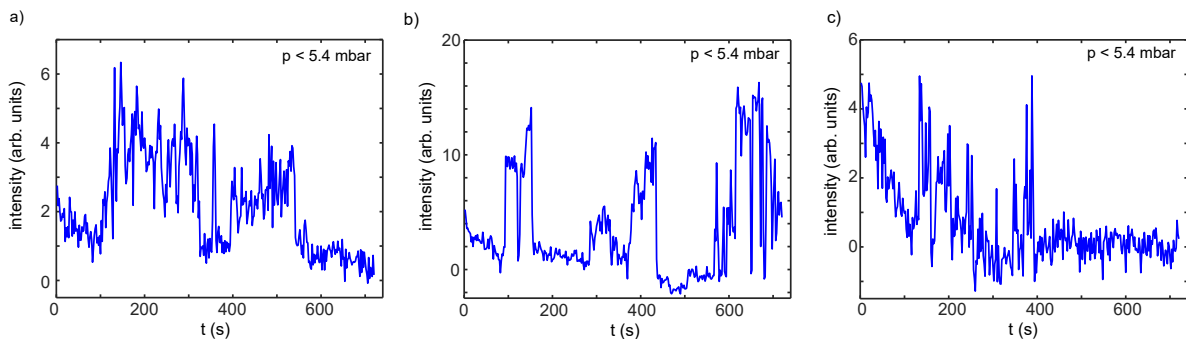


Figure S4: Examples of fluorescence blinking for single nanoantennas at low pressure (below 5.4 mbar) for three antennas. The blinking appears to be not modified when the pressure is reduced by factor of 250 from ambient conditions.

(black solid line).

## Vacuum

To exclude interaction of the GNRs with gas molecules from the environment as a source of the fluorescence blinking, we investigate the photoluminescence when the pressure is reduced from 1000 mbar to 4 mbar. We would expect a proportional decrease in the blinking events if interaction with gas molecules was the origin. The sample was kept inside a vacuum chamber. For these measurements the microscope objective was exchanged to a long working distance objective with a numerical aperture of 0.42 (LCD Plan NIR 50x, Mitutoyo). Even

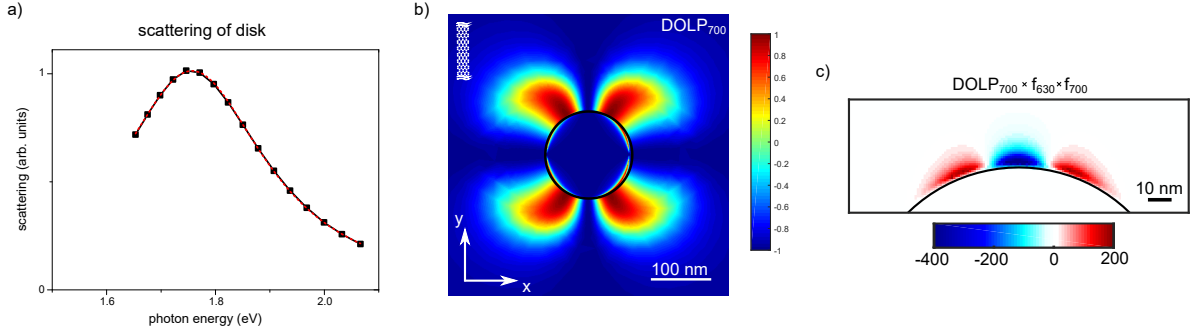


Figure S5: Simulations: a) calculated scattering spectrum for a single nanoantenna. b) Degree of linear polarization for the emission of a  $y$ -oriented dipole. Positive values indicate  $x$ -polarized emission. c) Polarization-weighted enhancement factor for  $y$ -oriented emitter (product of DOLP and enhancement factors for excitation and emission). Positive values indicate a rotation of the emission polarization, such that the signal in the perpendicular polarization channel is stronger than in the parallel.

with reduced pressure, we still observe fluorescence blinking as shown in three examples in Fig. S4a–c. Due to the reduced numerical aperture the separation of detected emission from individual antenna elements is not as good as for the results presented in the main text. This leads to larger time-dependent spatially varying fluctuations in the background of the blinking traces.

## Simulations

We perform full-field simulations using a finite element solver (Comsol Multiphysics). The enhancement of the emission is obtained by applying the Lorentz reciprocity theorem for an incident plane wave at normal incidence.<sup>3</sup> The total enhancement is obtained as the product of the excitation and emission enhancement factors at each point in the investigated sample plane. The calculations are performed for an incident wavelength of 630 nm and an emission wavelength of 700 nm, which correspond to the excitation wavelength used in the experiment and the center of the emission band, respectively.

To study the scattering properties of the structures, we evaluate the power of the to the far-field scattered fields around a nanoantenna when it is illuminated with a polarized plane

wave incident at normal incidence. For the geometry we consider the antennas as 70 nm radius and 30 nm high gold cylinders on a glass surface. For gold we use tabulated values for the wavelength dependent refractive index<sup>4</sup> while for substrate we use a constant refractive index of 1.5. The simulation domain boundaries are enclosed by perfectly matched layers. The calculated scattering spectrum is shown in Fig. S5a. From a Lorentzian fit we extract the resonance at a photon energy of 1.757 eV and a resonance width of 331 meV.

## Rotation of the emission polarization

To investigate the rotation of the polarization in the vicinity of the antennas, we calculate the degree of linear polarization (DOLP) for the emitted light. The DOLP is defined as

$$DOLP = \frac{S_{perp} - S_{par}}{S_{perp} + S_{par}}, \quad (1)$$

where  $S_{perp}$  is the collected emission polarized perpendicular and parallel  $S_{par}$  to the GNRs, respectively. We calculate the DOLP for emitters in a plane which is situated 2 nm above the antenna's top surface. For an emission wavelength of 700 nm (photon energy 1.771 eV) and an emitter, which is oriented along the GNR orientation direction, the DOLP as a function of the emitter position is shown in Fig. S5b. According to the definition above, positive DOLP values indicate signals where the perpendicularly polarized field components exceed the parallel. One observes four lobes, which signal rotation of the polarization. However, the DOLP is not dependent on the absolute magnitude of the signal. We therefore plot in Fig. S5c the product of the enhancement factors for emission and excitation (for an excitation wavelength of 630 nm and an emission wavelength of 700 nm) and the DOLP as a function of position in a plane 2 nm above the antennas. Here the sign indicates the dominating polarization component while the magnitude signifies the enhancement. The antenna's hot-spot appears split in three regions. The central region of the hot-spot exhibits large negative values, which indicate DOLP values close to -1 and large enhancement factors.

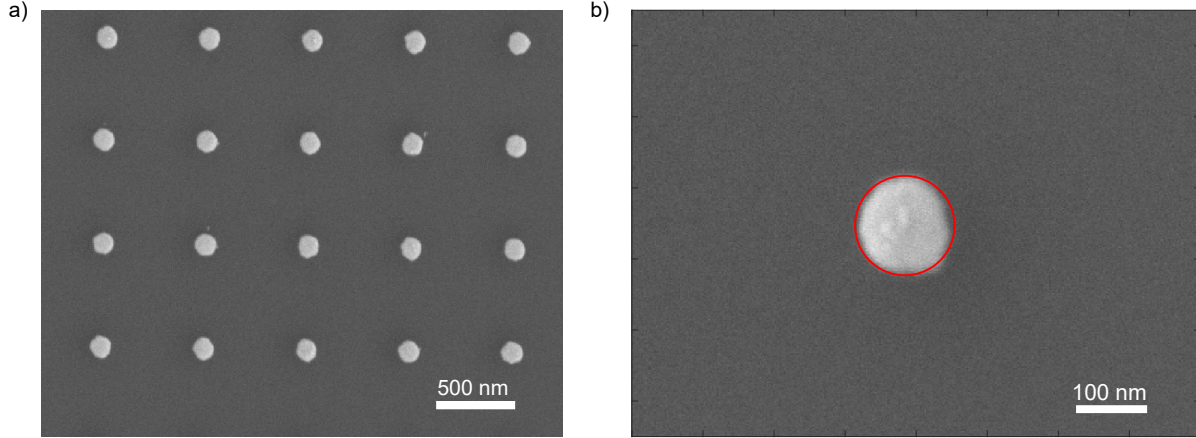


Figure S6: Scanning electron micrographs of optical antennas, which were fabricated under same conditions as the sample on which the optical experiments were measured. a) Overview of the sample. b) Closer view of a single antenna. The red solid line indicates a diameter of 140 nm, which was assumed for the finite element simulations.

This corresponds to enhanced emission polarized along the emitter dipole, i.e no rotation of the emission polarization. For the two lobes to the sides, the enhancement factors are large, yet, the DOLP is positive, which indicates a rotation of the emitted polarization direction. By comparison with Fig. 1b in the main text, in the transition between regions of positive and negative values the enhancement is large but the DOLP is equal to zero.

## Structures

We performed scanning electron microscopy on a sample which was fabricated under identical conditions as the one used for the optical experiments. The sample used for optical spectroscopy measurements was not scanned with an electron beam in order to avoid sample contamination. Scanning electron micrographs of the antennas are shown in Fig. S6. The disk diameter of 140 nm, indicated by the red solid line in panel b), was used for the finite element simulations.

# Power-law statistics of fluorescence blinking

## Single trace with short integration time

To obtain the power-law exponents of the blinking statistics we analyze a time-trace (see Fig. S7a) which is recorded on a single antenna. The emission is in this case detected using a fast single photon counting avalanche photo detector in the same microscope that is used in the other experiments. The time bins are binned from 20 ms to 60 ms to decrease the noise level. To a histogram of brightnesses, shown in Fig. S7b, we fit two Gaussian peaks. The peak corresponding to the low brightness values characterizes the brightness in the "off" state. The width of the this Gaussian  $\sigma$  therefore measures the spread in brightness when the emitter is dark. We use this to determine the threshold to separate the "on" and "off" states. We vary the threshold level from  $2\sigma$  to  $3\sigma^5$  in steps of  $0.1\sigma$ . For the shown trace, depending on the threshold level, we obtained at least 340 bursts. From the binary traces we generate histograms  $N_{on,i}(\Delta t_i)$  and  $N_{off,i}(\Delta t_i)$  of burst lengths and dark periods, respectively. For each obtained histogram we fit the power-law to a reduced dataset, where only short time bin points until the first vanishing value are included (marked with red points in Fig. 2a in the main text). For the fit procedure we apply a statistical error weighting, i.e. the error for the time bin  $\Delta t_i$  is scaled by  $1/N_i$ . The obtained exponents are shown in Fig. S7c. The resulting values for the "on"-times  $\alpha_{on}$  are between -1.70 and -1.50 and for the "off"-times  $\alpha_{off}$  between -1.75 and -1.5. The mean values are  $\alpha_{on} = -1.583$  and  $\alpha_{off} = -1.637$ . The threshold value within the chosen range thus does not influence the conclusions.

## Ensemble of traces with 1 s integration time

We additionally evaluate time traces for 56 antennas, each recorded over 400 s with an integration time of 1 s. The "on" and "off" time histograms are shown in Fig. S8a and b, respectively. The fitted power law exponents are  $\alpha_{on} = -1.687$  and  $\alpha_{off} = -1.675$  and are thus in good agreement with the exponents for shorter time intervals.

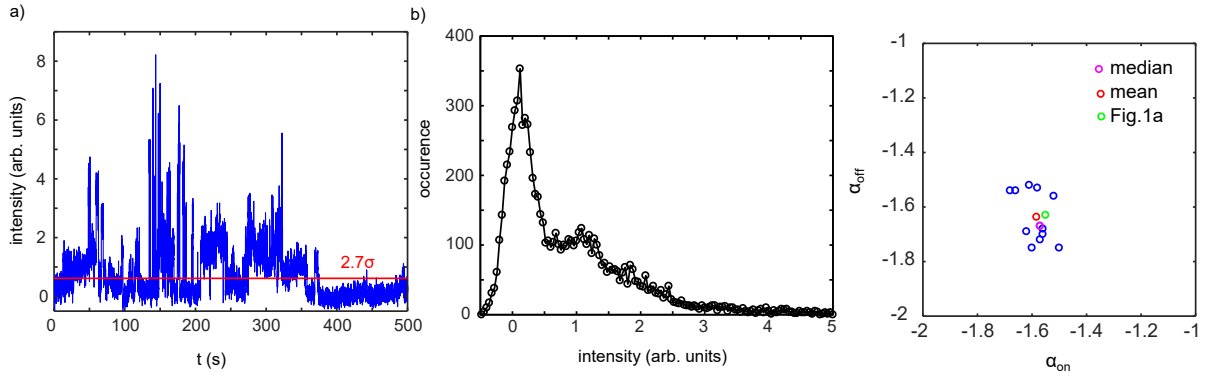


Figure S7: a) Time trace from one antenna. The threshold was set between 2 and 3  $\sigma$  above the background level. b) This is between the two peaks in the histogram of brightnesses. c) Fitted power-law exponents for on- and off time for different threshold levels.

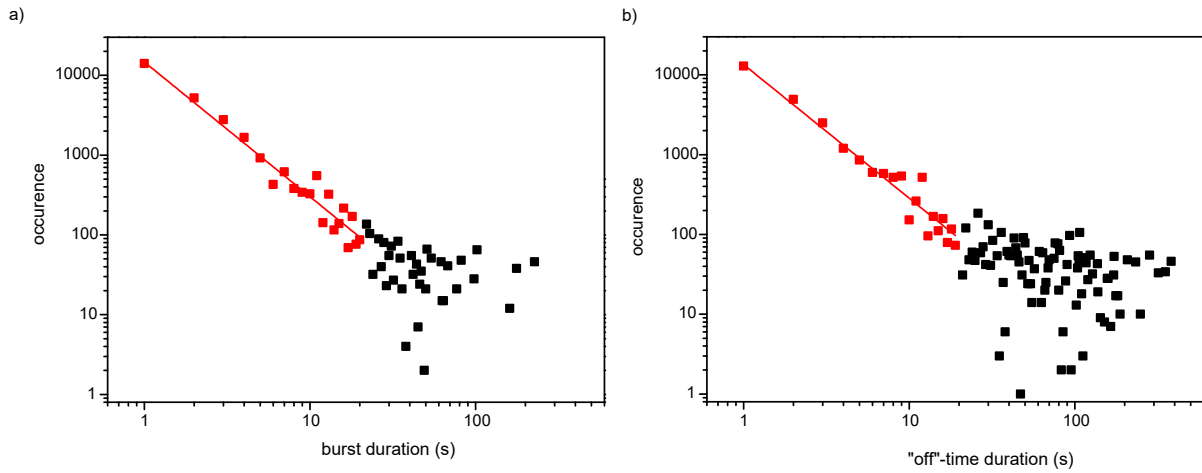


Figure S8: Histograms for "on" and "off" durations evaluated for 56 antennas for acquisition time of each 400 s [panels a) and b), respectively]. The fitted exponents are  $\alpha_{on} = -1.687$  and  $\alpha_{off} = -1.675$ .

## References

- (1) Chong, M. C.; Afsharimani, N.; Scheurer, F.; Cardoso, C.; Ferretti, A.; Prezzi, D.; Schull, G. Nano Letters **2018**, 18, 175–181.
- (2) Mugarza, A.; Mascaraque, A.; Pérez-Dieste, V.; Repain, V.; Rousset, S.; García de Abajo, F. J.; Ortega, J. E. Phys. Rev. Lett. **2001**, 87, 107601.
- (3) Carminati, R.; Nieto-Vesperinas, M.; Greffet, J.-J. J. Opt. Soc. Am. A **1998**, 15, 706–712.
- (4) Johnson, P. B.; Christy, R. W. Phys. Rev. B **1972**, 6, 4370.
- (5) Kuno, M.; Fromm, D. P.; Hamann, H. F.; Gallagher, A.; Nesbitt, D. J. The Journal of Chemical Physics **2001**, 115, 1028–1040.